This manuscript is a preprint and priory submitted for publication in **Journal of Hydrology**. Please note that this manuscript has not yet undergone peer-review; as such, subsequent version of this manuscript may have different content.

Title:

Retrieving Chl-a and total suspended solids in in-land waters using EnMAP simulated data

*Mohammadmehdi Saberioon**,
Corresponding author

Section 1.4 Remote Sensing and Geoinformatics, Helmholtz Centre Potsdam GFZ German Research Centre for Geosciences, Telegrafenberg, Potsdam 14473, Germany

saberioon@gfz-potsdam.de

Vahid Khosravi

Department of Soil Science and Soil Protection, Faculty of Agrobiology, Food and Natural Resources, Czech University of Life Sciences Prague, Kamycka 129, Suchdol, Prague 16500, Czech Republic

khosravi@af.czu.cz

Jakub Brom

Department of Applied Ecology, Faculty of Agriculture and Technology, University of South Bohemia in České Budějovice, Studentská 1668, České Budějovice 37005, Czech Republic

jbrom@fzt.jcu.cz

Asa Gholizadeh

Department of Soil Science and Soil Protection, Faculty of Agrobiology, Food and Natural Resources, Czech University of Life Sciences Prague, Kamycka 129, Suchdol, Prague 16500, Czech Republic

gholizadeh@af.czu.cz

Karl Segl

Section 1.4 Remote Sensing and Geoinformatics, Helmholtz Centre Potsdam GFZ German Research Centre for Geosciences, Telegrafenberg, Potsdam 14473, Germany

karl.segl@gfz-potsdam.de

Retrieving Chl-a and total suspended solids in in-land waters using EnMAP simulated data

Mohammadmehdi Saberioon[a,*], Vahid Khosravi[b], Jakub Brom[c], Asa Gholizadeh[b], Karl Segl[a]

[a]*Helmholtz Centre Potsdam GFZ German Research Centre for Geosciences, Section 1.4 Remote Sensing and Geoinformatics, Telegrafenberg, Potsdam 14473, Germany*
[b]*Department of Soil Science and Soil Protection, Faculty of Agrobiology, Food and Natural Resources, Czech University of Life Sciences Prague, Kamycka 129, Suchdol, Prague 16500, Czech Republic*
[c]*Department of Applied Ecology, Faculty of Agriculture and Technology, University of South Bohemia in České Budějovice, Studentská 1668, České Budějovice 37005, Czech Republic*

Abstract

The Environmental Mapping and analysis program (EnMAP) is a new Earth observation satellite which will use imaging spectroscopy to obtain a diagnostic characterisation of the Earth's surface and record changes. Since we hypothesis that imaging spectroscopy can significantly improve the accuracy of predicting and assessing water quality traits of small in-land waters, our study investigates the capability of the simulated EnMAP data to predict chlorophyll-a (Chl-a) and total suspended solids (TSS) as two of the most crucial water quality indicators. Three machine learning (ML) approaches(i.e., The methods used were Principal Component Regression(PCR), Partial Least Square Regression (PLSR) and Random Forest (RF)) were employed to establish links between the simulated image spectra and the above-mentioned water attributes of the samples collected from several in-land water reservoirs

*Corresponding author; email: saberioon@gfz-potsdam.de

within the southern part of the Czech Republic. Additionally, an airborne hyperspectral image likewise was used for developing a model to compare its performance with models developed based on simulated EnMAP data. According to the results, adequate prediction accuracy was obtained for Chl-a (RF: $R^2 = 0.89$, RMSE = 43.06, and LCCC = 0.91) and TSS (RF: $R^2 = 0.91$, RMSE = 17.53, and LCCC = 0.94), which was close enough to those obtained for the airborne hyperspectral image. Chl-a and TSS showed a correlation with around 550 and 650 nm and from 700 nm to 800 nm of the red and near-infrared (NIR) regions. The spatial distribution maps derived from the simulated EnMAP were comparable to those obtained by the source image, particularly in water bodies with relatively high and low contents of the water attributes. Overall, it can be concluded that the simulated EnMAP image was successful and reliable in the prediction and spatial mapping of the selected biophysical properties of the small in-land water bodies.
Keywords: Remote sensing, Satellite imagery, Hyperspectral imagery, Machine learning, Biophysical properties, Water quality

1. Introduction

In-land waters (i.e., water bodies with no direct sea or ocean connection) supply essential and diversified natural environment and ecological community services and support biodiversity while providing necessary water for various human applications (Stendera et al., 2012; Carvalho et al., 2013; Palmer et al., 2015; Dörnhöfer & Oppelt, 2016). However, human activities such as water extraction, wastewater discharge, spreading the invasive species, and source water interference have threatened the in-land water quality (Palmer et al., 2015; Maier & Keller, 2019).

Developing rapid, low-priced, and precise water quality monitoring and assessment schemes to avert destructive changes through timely treatments is essential. However, conventional point-based in-situ water monitoring plans have limited spatial and temporal variability coverage. In addition, they are time, cost, and labour demanding (Schaeffer et al., 2013) and yield non-representative and inaccurate water quality maps as a result of unevenly distributed single measurements (Van Puijenbroek et al., 2015).

Remote sensing (RS) has shown a remarkable ability for monitoring and assessment of in-land water bodies by extracting the water spectral information and transforming them into some quality parameters such as total suspended solids (TSS) (Guimarães et al., 2019; Saberioon et al., 2020; Du et al., 2022), turbidity (Keller et al., 2018; Cui et al., 2022; Rodríguez-López et al., 2021), microbiological properties such as chlorophyll a (Chl-a) (Keller et al., 2018; Saberioon et al., 2020; Silveira Kupssinskü et al., 2020; Gupana et al., 2021; Maier et al., 2021), and organic properties including dissolved organic carbon (DOC) and colored dissolved organic matter (CDOM) (Cao et al., 2018; Keller et al., 2018; Ross et al., 2019; Li et al., 2022), allowing exhaustive monitoring of in-land water bodies. These advantages have made RS an efficient water monitoring technique which can complement in-situ measurements.

Due to the finer spectral resolution of hyperspectral data, significant attention has been directed toward the hyperspectral RS. Based on acquisition platforms, three types of hyperspectral RS data have been used for in-land water quality monitoring: (i) satellite data such as Hyperion (Giardino et al.,

2007) and PRecursore IperSpettrale della Missione Applicativa (PRISMA) (Bresciani et al., 2022), (ii) airborne data such as HyMap (Thiemann & Kaufmann, 2002), Airborne Imaging Spectrometer for Applications (AISA) (Pyo et al., 2018; Vinciková et al., 2015), Airborne Spectrographic Imager (CASI) (Beck et al., 2016), and Airborne Prism Experiment (APEX) (Knaeps et al., 2015), and (iii) low altitude platforms acquired data (e.g., unmanned aerial vehicles (UAV)) (Guimarães et al., 2019; Cillero Castro et al., 2020). Most airborne- and UAV-based sensors record very high spatial resolution images without being affected by atmospheric distortions, but they lack temporal continuity since they usually do not operate regularly (Transon et al., 2018). On the contrary, satellite data is recorded automatically, regularly, and frequently with proper repetitive temporal coverage. However, due to some constraints such as high instrumental imaging and computation cost and low signal-to-noise ratio (SNR), the number of satellite missions with hyperspectral sensors is significantly lower than those carrying the multispectral ones (Govender et al., 2007). Launching new orbital hyperspectral satellites with higher spectral, spatial, temporal and radiometric resolution sensors will lead to more reachable and accurate water quality parameters retrieval and mapping.

The hyperspectral imager (HSI) Environmental Mapping and Analysis Program (EnMAP) is a German satellite mission for global scale monitoring of severe environmental challenges caused by climate change and human activities (Guanter et al., 2015). It was launched on 1st April 2022 with a swath width of 30 km, spatial resolution of 30 m, a radiometric resolution of 14 bits and four days of minimum temporal resolution using tilt angle observations. EnMAP products will consist of 218 bands covering a spectral range from 420 nm to 2450 nm, which we hypothesise that it has ability to detect Chl-a or other pigments in various circumstances (Saberioon et al., 2020). Furthermore, EnMAP covers both red and near infrared (NIR) regions with a relatively high SNR, making it an appropriate choice for remote estimation of water physicochemical properties (Ruddick et al., 2016).

Although empirical models developed for quantifying water quality traits through inversion of the nonlinear correlative relationship between water quality parameters and reflectance spectra within the red and NIR portion of the electromagnetic spectrum (Choubey, 1992; Goodin et al., 2008; Ouillon et al., 2008; Chen et al., 2007), they are vulnerable to seasonal and spatial differences. Therefore, Machine Learning (ML)-based approaches including Support Vector Machine (SVM) (Keller et al., 2018; Maier & Keller, 2019), Cubist (Saberioon et al., 2020), Random Forest (RF) (Silveira Kupssinskü et al., 2020; Rubin et al., 2021) , Artificial Neural Networks (ANN) (Silveira Kupssinskü et al., 2020; Maier & Keller, 2019), and Extreme Machine Learning (Peterson et al., 2018), became popular for developing semi-empirical models. They provide intelligent ways of eliminating irrelevant spectral wavelengths while unravelling the complex relationship between response and predictor variables with limited assumption and prior knowledge (Saberioon et al., 2020; Chen et al., 2022).

In this context, this study aims to assess the capacity of spectral information provided by EnMAP for quantifying and mapping Chl-a and TSS, as two important in-land water quality traits. Additionally, Results are compared with those Chl-a and TSS values obtained directly by airborne image spectra. The investigation also includes the development of ML models for assessing Chl-a and TSS, which may offer critical information on these water quality metrics in a more accurate, rapid, and less computational-demanding manner than the existing methods.

2. Materials and Methods

2.1. Test sites, water sampling, and variable measurements

The area of interest is located in the Třeboň Basin Biosphere Reserve, South Bohemia, Czech Republic. It is a historical area that is relatively flat, with a large number of ponds and artificial water reservoirs. These cover up to 15 % of the area. The history of some of the ponds goes back several centuries. The altitude is around 420 m above sea level. The mean annual temperature varies by about 7.8 °C, and the annual sum of precipitation is circa 650 mm. The ponds are shallow turbid reservoirs primarily intended for the commercial breeding of carp (*Cyprinus carpio* L.) or other freshwater fish. The depth of the ponds does not usually exceed 3 m; the area varies from hundreds of square metres up to 648 ha (Rožmberk fishpond). Most of the ponds in the area have eutrophic to hypertrophic character with high turbidity and low water transparency (tens of centimetres). There are also oligotrophic to mesotrophic reservoirs in the area with low turbidity and high water transparency (approx. 1 m). These are mainly sandpits with depths of up to 30 m. These lakes are currently used mostly for recreation and partly for mining. A map of the area of interest is shown in Figure 1.

Water samples for laboratory analyses were collected during the aerial imaging campaign on July 11, 2010. Water samples were collected at reser-

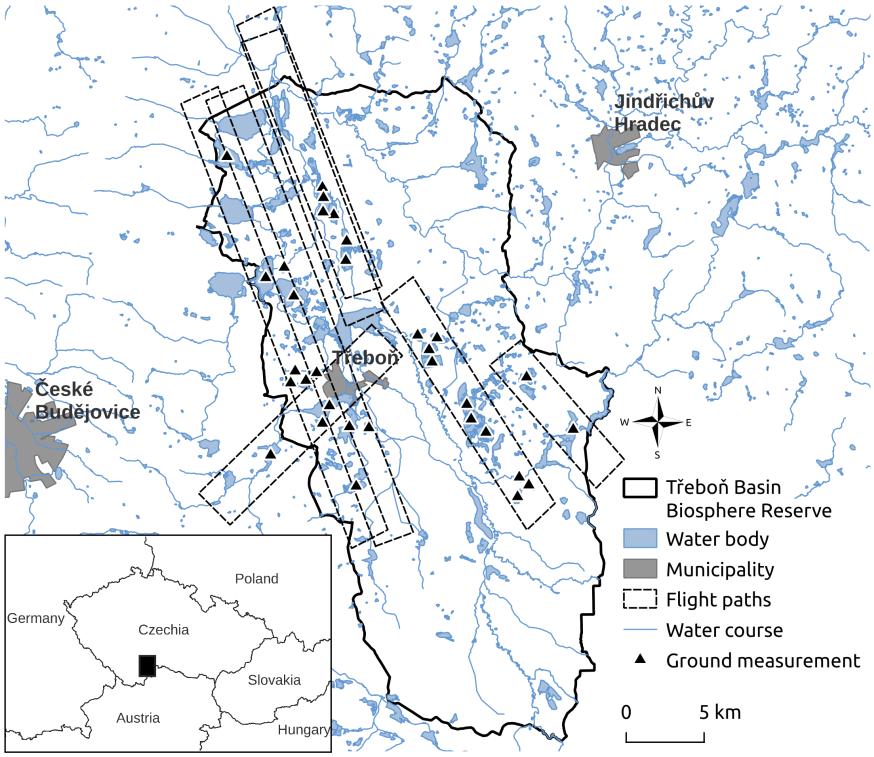

Figure 1: Area of interest map with highlighted flight paths and water sampling points. Aerial hyperspectral imaging was performed on 11 July 2010.

voirs with different trophic levels, i.e., hypertrophic ponds and sandpit lakes with oligotrophic-mesotrophic water types. Each sampling point was recorded using a GPS tracker. The samples collected were analysed in the laboratory immediately after collection. Chl-a values were estimated by reading of absorbance with double beam UV–Vis spectrophotometer Heλios Alpha (Unicam, GB) at 664 nm after extraction with a mixture of 90 % acetone:methanol (Pechar, 1987). TSS was determined as dry weight of seston captured on pre-weighed Whatman GF/C filters and dried to constant weight at 60 ºC (Vinciková et al., 2015).

2.2. Hyperspectral airborne imaging spectrometers data acquisition and preprocessing

Aerial measurements were performed using the AISA Eagle airborne hyperspectral imaging system (Specim Ltd, Finland). The spectral range was 400 to 1000 nm with a spectral resolution of 2.2 nm. Within the seven flight paths, 260 spectral bands were acquired (see Figure 1). The spatial resolution of the hyperspectral images was 5.5 m. The hyperspectral data were acquired between 09:30 and 11:30 central Europe time (CET) on 11 July 2010. The ASD FieldSpec-3 spectroradiometer was used to measure the optical properties of the reference surfaces. These supportive data were used for images calibration and validation. Microtops II Sunphotometer measurements were used to estimate the current atmospheric conditions, aerosol optical thickness (AOT) and water vapour (WV). Preprocessing of the AISA Eagle data acquired during the flight campaign was performed in CaliGeo (radiometric corrections), PARGE (orthorectification) and ATCOR-4 (atmospheric corrections) software. The hyperspectral image data were georeferenced to the WGS84/UTM Zone 33N (EPSG 32633) coordinate system. For further details see (Hanuš et al., 2008).

2.3. Simulation of EnMAP spaceborne hyperspectral image

EnMAP data and associated radiance and reflectance products (Level 1B/1C/2A) were generated using the EnMAP end-to-end simulation software EeteS (Segl et al., 2012). EeteS is an instrument simulator developed to support EnMAP mission preparatory activities. The sequential processing chain of the software consists of four independent modules - the atmospheric, spatial, spectral and radiometric modules, in which hyperspectral reflectance data is used to calculate top-of-atmosphere radiance and subsequently digital numbers (L0). This forward simulator is coupled with a backward simulation branch consisting of sensor calibration modules and a complete L1/L2 preprocessing chain. As a result, a realistic EnMAP scene with 30 m pixel resolution and 242 spectral bands ranging between 420 nm and 2450 nm was generated.

2.4. Quantitative modeling and prediction assessment

Three modeling approaches were used to predict the water parameters: Principal Component Regression (PCR), Partial Least Square Regression (PLSR) and RF. All techniques are appropriate when observations are limited and more predictors are available and they have been reportedly used in the analysis of the hyperspectral RS data water properties (Song et al., 2012; Sudduth et al., 2015; Wang et al., 2020; Flores et al., 2021).

PCR is a linear regression model obtained by combining the multiple linear regression (MLR) and principal component analysis (PCA) to suppress the problem of MLR methods facing the multicollinearity between variables (Liu et al., 2003). PLSR is another linear regression method that projects independent variables (X) as predictors and dependent variables (Y) as responses into a set of orthogonal latent factors while maximising the covariance between X- and Y-scores (Wold et al., 2001). In RF, as an ensemble learning method, decision trees are trained and then a voting procedure is employed to combine the result obtained by each tree. Unlike the noise sensitivity of every single tree's prediction outcome, uncorrelated trees combination will not yield that much noisy results. Furthermore, training data will be created by bagging approach –drawing sample subsets with replacement–

which may cause improved model performance (Belgiu & Drăguţ, 2016).

Water samples were divided into calibration and testing (75 % and 25 % respectively) sets randomly. Prediction models were trained on the calibration set using 5-repeated 10-fold cross-validation, while their generalisation capability was evaluated on the test set. The coefficient of determination (R^2), root mean square error (RMSE), Lin's concordance correlation coefficient (LCCC) and bias were used to assess the performance of the models in calibration, validation and testing steps.

2.5. Chl-a and TSS spatial distribution mapping

The best prediction models were applied to both image pixels' spectra and Chl-a and TSS distribution maps of water bodies were produced by linear Triangulated Irregular Network (TIN) interpolation with grid 10 m in QGIS 3.22 environment. Finally, the spatial patterns of water properties obtained by AISA Eagle hyperspectral airborne and simulated EnMAP data were compared.

3. Results

3.1. Statistical description of Chl-a and TSS

The water properties box-plots and QQ-plots are shown in Figure 2. As can be seen, one Chl-a value was considered as outlier, while TSS contents of the samples did not include any outlier.

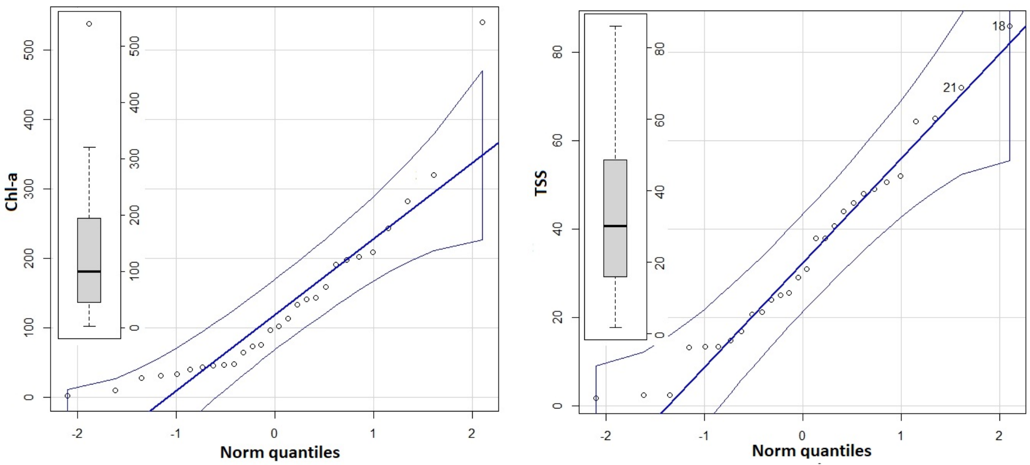

(a) (b)

Figure 2: QQ-plots and box-plots of (a) Chl-a and (b) TSS

General statistics of Chl-a and TSS contents of water samples, namely minimum (Min), maximum (Max), mean, standard deviation (SD), coefficient of variation (CV), and skewness, were calculated after removing the sample with outlier value of Chl-a (Table 1). Accordingly, compared to TSS, Chl-a showed more variability due to the wider range of data, which was reflected in its coefficient of variation value (76.96%), which indicates a more heterogeneous distribution of Chl-a in comparison to the TSS.

Table 1: Descriptive statistics of Chl-a (μg/L) and TSS (mg/L)

Parameter	Min	Max	Mean	SD	Skewness	CV (%)
Chl-a	2.23	320.44	114.08	86.66	1.62	76.96
TSS	1.75	86	33.88	21.52	0.46	63.5

3.2. Correlation of Chl-a and TSS with reflectance spectra

Pearson correlation analysis was used to explore the correlation between Chl-a and TSS contents in the in-land water and the spectra of both hyperspectral images (i.e., AISA Eagle airborne hyperspectral imaging system and simulated EnMAP) in the range between 420 nm and 980 nm. It can be observed (Figure 3) that both Chl-a and TSS highly correlated with spectral wavelengths around 550 nm, 660 nm and also in the red and NIR region from 700 nm to 800 nm. The maximum correlation values relating to Chl-a were obtained with the spectra from simulated EnMAP at about 710 nm, while TSS content and airborne image spectra had their highest correlation at about 800 nm.

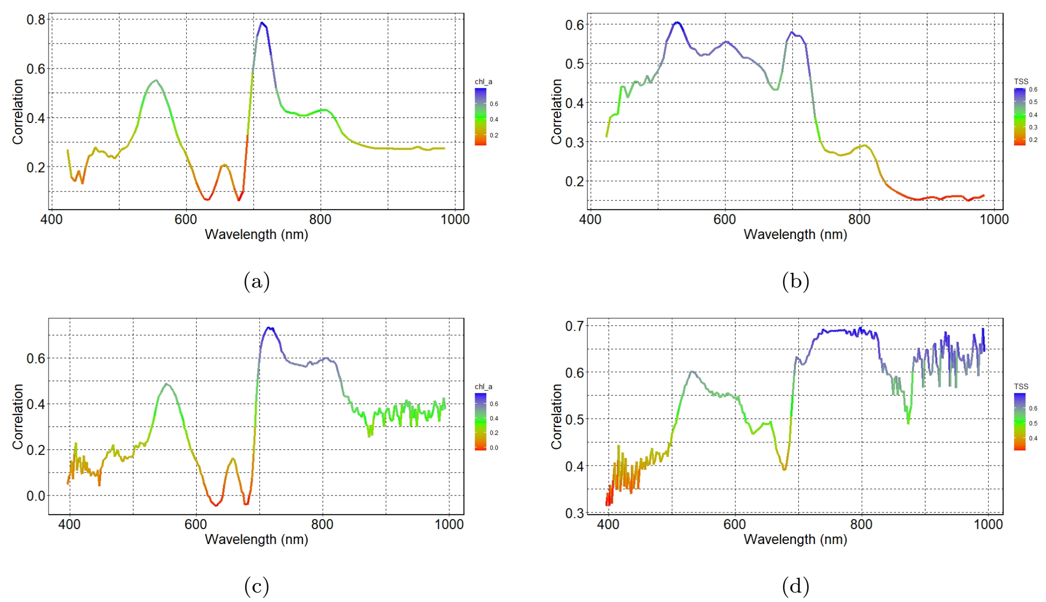

Figure 3: Correlation between the simulated EnMAP pixels spectra and (a) Chl-a, (b) TSS and AISA Eagle airborne hyperspectral image pixels spectra and (c) Chl-a and (d) TSS

3.3. Performance of Chl-a and TSS prediction models

Chl-a and TSS prediction results using both types of RS data (AISA Eagle airborne and simulated EnMAP) are presented in Table (2).

Table 2: Performance of Chl-a and TSS prediction models developed by PCR, PLSR, and RF

			Airborne				EnMAP			
Properties	Method	Dataset	R^2	RMSE	LCCC	bias	R^2	RMSE	LCCC	bias
Chl-a	PCR	Calibration	0.96	26.24	0.97	-1.55	0.90	56.3	0.93	-3.11
		Validation	0.88	31.95	0.91	-13.71	0.85	59.11	0.89	-18.43
		Test	0.79	53.76	0.84	23.44	0.64	64.67	0.68	40.43
	PLSR	Calibration	0.94	33.08	0.95	0.3	0.92	47.09	0.95	-1.05
		Validation	0.89	48.63	0.92	-12.16	0.87	54.15	0.91	21.05
		Test	0.83	50.34	0.87	25.28	0.69	62.99	0.74	34.72
	RF	Calibration	0.95	29.53	0.98	0.1	0.92	39.88	0.96	2.05
		Validation	0.93	31.82	0.96	-5.36	0.89	40.75	0.95	19.82
		Test	0.91	34.23	0.93	-10.97	0.89	43.06	0.91	33.01
TSS	PCR	Calibration	0.90	8.89	0.91	-0.07	0.88	9.72	0.91	-1.81
		Validation	0.83	11.54	0.88	-10.45	0.81	20.48	0.85	21.05
		Test	0.77	13.39	0.81	-16.32	0.71	29.92	0.72	37.38
	PLSR	Calibration	0.93	7.48	0.95	0.08	0.86	10.94	0.92	-0.56
		Validation	0.87	11.92	0.90	-5.81	0.85	16.22	0.89	9.63
		Test	0.81	18.17	0.84	-7.41	0.75	21.39	0.78	23.44
	RF	Calibration	0.97	8.37	0.99	0.43	0.95	9.16	0.97	1.05
		Validation	0.96	10.36	0.97	3.49	0.93	14.92	0.96	-8.34
		Test	0.94	13.76	0.96	-5.12	0.91	17.53	0.94	11.43

Regarding the applied ML method, different results were obtained for different Chl-a and TSS. The best Chl-a prediction was obtained using RF with R_p^2= 0.91, $RMSE_p$= 34.23 μg/L, LCCC = 0.93 and bias = -10.97 on the AISA Eagle airborne data (Figure 4a) and R_p^2 = 0.89, $RMSE_p$ = 43.06 μg/L, LCCC = 0.91 and bias = 33.01 for the simulated EnMAP (Figure 4c). Similarly, TSS was best predicted by RF (R_p^2 = 0.94, $RMSE_p$= 13.76 mg/L, LCCC = 0.96 and bias = -5.12) applied on the AISA Eagle airborne image (Figure 4b). The simulated EnMAP and RF estimated TSS with R_p^2 = 0.91, $RMSE_p$ = 17.53 mg/L, LCCC = 0.94 and bias = 11.43 (Figure 4d).

The results highlights that though both water properties were acceptably assessed, TSS was predicted with a higher accuracy than Chl-a.

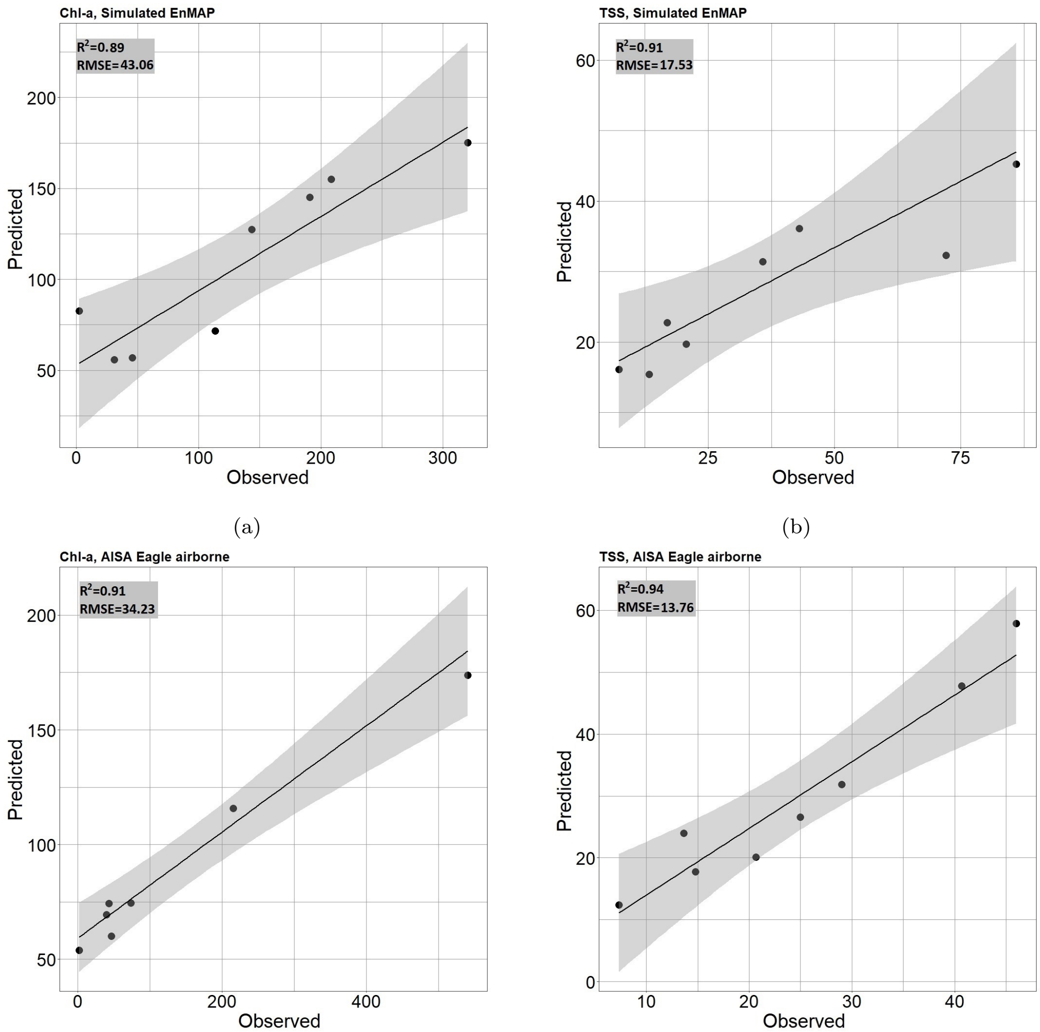

(a) (b) (c) (d)

Figure 4: The measured versus RF-predicted values of Chl-a using (a) simulated EnMAP and (c) AISA Eagle airborne images, and TSS using (b) simulated EnMAP and (d) AISA Eagle airborne images (test dataset)

As Expected, regardless of the water parameter, all prediction methods (PCR, PLSR, and RF) yielded better results for the AISA Eagle airborne image. This superiority was achieved for calibration, validation, and test datasets. Conversely, the prediction results derived from the simulated EnMAP were acceptable too (Table 2). This highlights that the images from simulated EnMAP were suitable for predicting Chl-a and TSS in this study area.

3.4. Spatial distribution maps of Chl-a and TSS

The spatial distribution maps of the water quality indicators estimated using the AISA Eagle airborne hyperspectral and EnMAP simulated images are shown in Figure 5. Both images yielded similar patterns for Chl-a and TSS in the water bodies under study. The spatial distribution of Chl-a content is similar for both data types (5 a) and c)). The AISA image shows relatively lower values of Chl-a content than the image from the simulated EnMAP data. The images also show that the AISA sensor data show more detail, which is due to the spatial resolution of the original data. The high Chl-a values at the edges of the reservoirs marked by green vegetation belong to the littoral vegetation.

The TSS values also have the same spatial distribution in both images (5 b) and d)). The values obtained from the simulated EnMAP data are slightly higher.

Within the study area, there are differences in Chl-a and TSS content between the different reservoirs. This is mainly due to the management of each reservoir and nutrient inputs from the catchment.

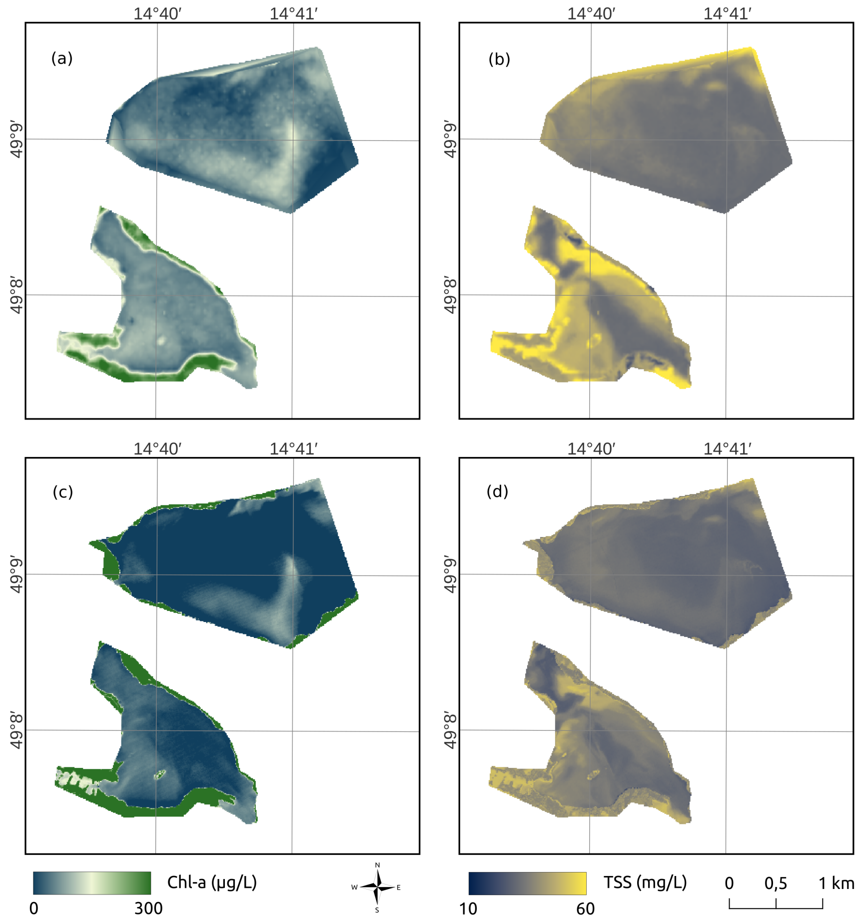

Figure 5: Spatial distribution of Chl-a and TSS in selected fishponds obtained from simulated EnMAP (top row) and AISA Eagle airborne hyperspectral imagery (bottom row)

Discussion

To study ecological, environmental and hydrological processes, it is essential to estimate water dynamics and quality of inland waters; however, it is challenging as they are complex, dynamic and heterogeneous. Despite the significant progress made in remote sensing of water bodies and the promising performance of satellite data for estimating water quality traits, there are still some limitations, such as low spectral, the spatial or temporal resolution of current available multispectral sensors prevent us from taking advantage of remote sensing data fully. However, emerging new sensors such as EnMAP, which have higher resolutions, permit us to accurately monitor water dynamics and water qualities for the long term. The results of this study show that Chl-a and TSS contents of in-land water bodies can be quantitatively predicted (Table 2) and mapped (Figure 5)using the simulated EnMAP spectra. In other words, EnMAP can provide enough data to reasonably predict and visualize spatial distribution of Chl-a and TSS in small inland waters. The strong correlation of the Chl-a and TSS with the red and NIR wavelengths of 660 nm and 700–800 nm (Figure 3), which was seen in this study, is in a good agreement with several other literature. Kim et al. (2020) reported three key wavelengths (i.e., 662 nm, 702 nm, and 752 nm) with the highest correlation to estimate Chl-a concentration in a pond. A very high correlation of about 0.8 has also been reported between Chl-a content of a lake and in-situ hyperspectral data at 719 nm in a study conducted by Jiao et al. (2006). Similarly, a high correlation between Chl-a and hyperspectral data was found at about 700 nm in the study of retrieving Chl-a concentrations in coastal waters readlized by Ryan & Ali (2016). Saberioon et al. (2020) also reported that both Chl-a and TSS had the highest correlations with Sentinel-2 band 5 (698–713 nm, Central wavelength 703 nm) for inland waters. In addition, Sentinel-2 band 5 also showed the highest correlation with turbidity of lakes water in northeastern China (Ma et al., 2021). These strong correlations can be attributed to chlorophyll absorbance at 670 nm and other plant pigment absorption peaks at 593 and 620nm (Gitelson et al., 1996; Sagan et al., 2020).

In terms of TSS, Wu et al. (2014) showed that NIR region (750–900 nm) could yield the best relationship for the prediction of TSS and turbidity in fresh water rivers. Bhargava & Mariam (1990) demonstrated that 700 nm to 900 nm was the optimal wavelength range for measuring suspended sediment concentrations. Furthermore, several other studies reported high correlation values between TSS and similar spectral regions (Novo et al., 1991; Han & Rundquist, 1994; Ma & Dai, 2005; Cao et al., 2021). These strong correlations can be ascribed to scattering peak in the red and NIR range of phytoplanktons and other organic and inorganic suspended materials at 700 nm (Olmanson et al., 2013; Sagan et al., 2020).

Few studies have explored the relationships between Chl-a and TSS concentrations and optical properties using details wavelengths other than the spectra in red and NIR ranges, similar to what we have conducted in this study by employing a whole VIS-NIR range hyperspectral data. Using the simulated EnMAP spectra, better results were obtained for both Chl-a (R_p^2 =0.89 , $RMSE_p$ = 43.06) and TSS (R_p^2 = 0.91, $RMSE_p$ = 17.53) (Table 2) than those of shown in an earlier study by Saberioon et al. (2020) on the same study area using the combination of Sentinel-2A bands and spectral indices (i.e., Chla: $R_p^2 = 0.85$, $RMSE_p = 49.63$; TSS: $R_p^2 = 0.8$, $RMSE_p = 19.55$). This can be mainly linked to higher spectral resolution and contribution of other effective wavelengths in prediction model. The supremacy of hyperspectral data over multispectral Sentinel-2 images has been reported in other studies too ((Awad, 2014; Sagan et al., 2020; Chen et al., 2022)).

Considering (Figure 4), RF performed well in determination of Chl-a and

TSS using both AISA eagle airborne hyperspectral and simulated EnMAP spectra. Furthermore, Table 2 highlights that RF outperformed PCR and PLSR in prediction of both Chl-a and TSS. This can principally be attributed to ability of RF to extract variables and interpret nonlinear relationship compared to PLSR and PCR (Ma et al., 2021). In addition, RF has the capability to handle data with small number and high dimensionality. The superiority of RF over other ML methods of predicting water quality traits from inland waters has also been reported in some other studies (Ma et al., 2021; Silveira Kupssinskü et al., 2020).

A visual comparison of the calculated Chl-a and TSS images shows similar values for the EnMAP simulated data and the AISA Eagle sensor (5). In the case of the AISA Eagle sensor, the high and low Chl-a values are highlighted. Lower values are likely underestimated in the AISA image, whereas the values from the simulated EnMAP data correspond better to typical Chl-a levels for this type of reservoirs. The calculated TSS values differ slightly, higher values were observed in case of EnMAP simulated data. The spatial pattern of the calculated values is similar for both sensors. More spatial heterogeneity is evident in the case of the AISA Eagle data. The different spatial patterns are mainly due to the spatial resolution of the data used.

Conclusions

This study evaluate the ability of EnMAP simulated data coupled with machine learning algorithms to predict two critical water quality properties for inland waters (i.e., Chl-a and TSS). To this end, Water samples were collected from several lakes and ponds in the south of the Czech republic concurrent to the hyperspectral AISA Eagle airborne imaging campaign. EnMAP simulation data also was generated based on the AISA Eagle airborne data using EeteS. As it demonstrated, the enhanced spectral resolution of EnMAP permitted the prediction of biochemical properties of small inland waters with acceptable accuracy. Additionally, results indicating that Vis/NIR hyperspectral imaging from orbit combined with machine learning algorithms has the potential to be used as a rapid and accurate method for predicting and mapping the water quality traits in small inland waters. From the point of view of practical applications (e.g. water resources managers, fishponds managers, nature conservation authorities etc.), the EnMAP simulated data provide sufficiently accurate information, both in terms of the accuracy of the determination of values and their spatial characteristics.

As actual EnMAP data will be available soon, the subsequent study will examine actual data's capacity for predicting water quality traits in small inland waters from orbit. Furthermore, evaluating the application of different spectral unmixing to decompose the optical water components seems necessary for small inland waters practically when we are dealing with hyperspectral data (Alcantara et al., 2009; Kwon et al., 2022).

Other ML algorithms, in general and deep learning algorithms ,in particular, can be applied to hyperspectral data to predict the water quality parameters with better accuracy and performance using orbital hyperspectral data. The number and spatial distribution of the samples, as well as influence of different atmospheric correction algorithm (Vanhellemont & Ruddick, 2021) are among important parameters that should be noticed in all future studies to create a representative dataset and make a ML-based model with acceptable generalisation (Menezes de Souza et al., 2020). As ML methods are prone to over-fitting and the curse of dimensionality, decreasing the feature space dimension using intelligent feature selection techniques can be another interesting topic of study. Furthermore, Increasing the number of trees does not cause over-fitting of the RF models (Breiman, 2001), which means better generalizability. Since the capability of our obtained model has not been proved yet, future studies can dedicate to testing it in other areas.

Acknowledgement

The authors would like to thank the EU, German's Federal ministry of education and research (BMBF) and The Technology Agency of the Czech Republic (TAČR) for funding, in the frame of the collaborative international consortium AIHABs financed under the ERA-NET AquaticPollutants Joint Transnational Call (GA Nº 869178). This ERA-NET is an integral part of the activities developed by the Water, Oceans and AMR Joint Programming Initiatives.

References

Alcantara, E., Barbosa, C., Stech, J., Novo, E., & Shimabukuro, Y. (2009). Improving the spectral unmixing algorithm to map water turbidity distributions. *Environmental Modelling & Software*, *24*, 1051 – 1061. doi:10.1016/j.envsoft.2009.02.013.

Awad, M. (2014). Sea water chlorophyll-a estimation using hyperspectral images and supervised artificial neural network. *Ecological informatics*, *24*, 60–68. doi:10.1016/j.ecoinf.2014.07.004.

Beck, R., Zhan, S., Liu, H., Tong, S., Yang, B., Xu, M., Ye, Z., Huang, Y., Shu, S., Wu, Q. et al. (2016). Comparison of satellite reflectance algorithms for estimating chlorophyll-a in a temperate reservoir using coincident hyperspectral aircraft imagery and dense coincident surface observations. *Remote Sensing of Environment*, *178*, 15–30. doi:10.1016/j.rse.2016.03.002.

Belgiu, M., & Drăguţ, L. (2016). Random forest in remote sensing: A review of applications and future directions. *ISPRS journal of photogrammetry and remote sensing*, *114*, 24–31. doi:10.1016/j.isprsjprs.2016.01.011.

Bhargava, D., & Mariam, D. W. (1990). Spectral reflectance relationships to turbidity generated by different clay materials. *Photogrammetric Engineering and Remote Sensing*, *56*, 225–229.

Breiman, L. (2001). Random forests. *Machine learning*, *45*, 5–32.

Bresciani, M., Giardino, C., Fabbretto, A., Pellegrino, A., Mangano, S., Free, G., & Pinardi, M. (2022). Application of new hyperspectral sensors in the remote sensing of aquatic ecosystem health: Exploiting prisma and desis for four italian lakes. *Resources*, *11*, 8. doi:0.3390/resources11020008.

Cao, F., Tzortziou, M., Hu, C., Mannino, A., Fichot, C. G., Del Vecchio, R., Najjar, R. G., & Novak, M. (2018). Remote sensing retrievals of colored dissolved organic matter and dissolved organic carbon dynamics in north american estuaries and their margins. *Remote sensing of Environment*, *205*, 151–165. doi:10.1016/j.rse.2017.11.014.

Cao, H., Han, L., Li, W., Liu, Z., & Li, L. (2021). Inversion and distribution of total suspended matter in water based on remote sensing images—a case study on yuqiao reservoir, china. *Water Environment Research*, *93*, 582–595. doi:`https://doi.org/10.1002/wer.1460`.

Carvalho, L., McDonald, C., de Hoyos, C., Mischke, U., Phillips, G., Borics, G., Poikane, S., Skjelbred, B., Solheim, A. L., Van Wichelen, J. et al. (2013). Sustaining recreational quality of european lakes: minimizing the health risks from algal blooms through phosphorus control. *Journal of Applied Ecology*, *50*, 315–323. doi:`10.1111/1365-2664.12059`.

Chen, J., Chen, S., Fu, R., Li, D., Jiang, H., Wang, C., Peng, Y., Jia, K., & Hicks, B. J. (2022). Remote sensing big data for water environment monitoring: Current status, challenges, and future prospects. *Earth's Future*, *10*, e2021EF002289. doi:`10.1029/2021EF002289`.

Chen, Z., Hu, C., & Muller-Karger, F. (2007). Monitoring turbidity in tampa bay using modis/aqua 250-m imagery. *Remote sensing of Environment*, *109*, 207–220. doi:`10.1016/j.rse.2006.12.019`.

Choubey, V. (1992). Correlation of turbidity with indian remote sensing satellite-1a data. *Hydrological sciences journal*, *37*, 129–140. doi:`10.1080/02626669209492573`.

Cillero Castro, C., Domínguez Gómez, J. A., Delgado Martín, J., Hinojo Sánchez, B. A., Cereijo Arango, J. L., Cheda Tuya, F. A., & Díaz-Varela, R. (2020). An uav and satellite multispectral data approach to monitor water quality in small reservoirs. *Remote Sensing*, *12*, 1514. doi:10.3390/rs12091514.

Cui, M., Sun, Y., Huang, C., & Li, M. (2022). Water turbidity retrieval based on uav hyperspectral remote sensing. *Water*, *14*, 128. doi:10.3390/w14010128.

Dörnhöfer, K., & Oppelt, N. (2016). Remote sensing for lake research and monitoring–recent advances. *Ecological Indicators*, *64*, 105–122. doi:10.1016/j.ecolind.2015.12.009.

Du, Y., Song, K., Wang, Q., Li, S., Wen, Z., Liu, G., Tao, H., Shang, Y., Hou, J., Lyu, L. et al. (2022). Total suspended solids characterization and management implications for lakes in east china. *Science of The Total Environment*, *806*, 151374. doi:10.1016/j.scitotenv.2021.151374.

Flores, H., Lorenz, S., Jackisch, R., Tusa, L., Contreras, I. C., Zimmermann, R., & Gloaguen, R. (2021). Uas-based hyperspectral environmental monitoring of acid mine drainage affected waters. *Minerals*, *11*, 182. doi:10.3390/min11020182.

Giardino, C., Brando, V. E., Dekker, A. G., Strömbeck, N., & Candiani, G. (2007). Assessment of water quality in lake garda (italy) using hyperion. *Remote Sensing of Environment*, *109*, 183–195. doi:10.1016/j.rse.2006.12.017.

Gitelson, A. A., Merzlyak, M. N., & Lichtenthaler, H. K. (1996). Detection of red edge position and chlorophyll content by reflectance measurements near 700 nm. *Journal of plant physiology*, *148*, 501–508. doi:10.1016/S0176-1617(96)80285-9.

Goodin, D. G., Harrington Jr, J. A., Nellis, M. D., & Rundquist, D. C. (2008). Mapping reservoir turbidity patterns using spot-hrv data. *Remote sensing images & technical notes*, (pp. 71–78). doi:10.1080/10106049609354563.

Govender, M., Chetty, K., & Bulcock, H. (2007). A review of hyperspectral remote sensing and its application in vegetation and water resource studies. *Water SA*, *33*, 145–151. doi:10.4314/wsa.v33i2.49049.

Guanter, L., Kaufmann, H., Segl, K., Foerster, S., Rogass, C., Chabrillat, S., Kuester, T., Hollstein, A., Rossner, G., Chlebek, C., Straif, C., Fischer, S., Schrader, S., Storch, T., Heiden, U., Mueller, A., Bachmann, M., M?hle, H., M?ller, R., Habermeyer, M., Ohndorf, A., Hill, J., Buddenbaum, H., Hostert, P., van der Linden, S., Leitáo, P. J., Rabe, A., Doerffer, R., Krasemann, H., Xi, H., Mauser, W., Hank, T., Locherer, M., Rast, M., Staenz, K., & Sang, B. (2015). The enmap spaceborne imaging spectroscopy mission for earth observation. *Remote Sensing*, *7*, 8830–8857. doi:10.3390/rs70708830.

Guimarães, T. T., Veronez, M. R., Koste, E. C., Souza, E. M., Brum, D., Gonzaga, L., & Mauad, F. F. (2019). Evaluation of regression analysis and neural networks to predict total suspended solids in water bodies from unmanned aerial vehicle images. *Sustainability*, *11*, 2580. doi:10.3390/su11092580.

Gupana, R. S., Odermatt, D., Cesana, I., Giardino, C., Nedbal, L., & Damm,

A. (2021). Remote sensing of sun-induced chlorophyll-a fluorescence in inland and coastal waters: Current state and future prospects. *Remote Sensing of Environment*, *262*, 112482. doi:10.1016/j.rse.2021.112482.

Han, L., & Rundquist, D. C. (1994). The response of both surface reflectance and the underwater light field to various levels of suspended sediments: preliminary results. *Photogrammetric Engineering and Remote Sensing*, *60*, 1463–1471.

Hanuš, J., Malenovský, Z., Homolová, L., Kaplan, V., Lukeš, P., & Cudlín, P. (2008). Potentials of the VNIR airborne hyperspectral system AISA Eagle. In *GIS Ostrava* (pp. 1–6). Ostrava, Czech Republic volume 27.

Jiao, H., Zha, Y., Gao, J., Li, Y., Wei, Y., & Huang, J. (2006). Estimation of chlorophyll-a concentration in lake tai, china using in situ hyperspectral data. *International Journal of Remote Sensing*, *27*, 4267–4276. doi:10.1080/01431160600702434.

Keller, S., Maier, P. M., Riese, F. M., Norra, S., Holbach, A., Börsig, N., Wilhelms, A., Moldaenke, C., Zaake, A., & Hinz, S. (2018). Hyperspectral data and machine learning for estimating cdom, chlorophyll a, diatoms, green algae and turbidity. *International journal of environmental research and public health*, *15*, 1881. doi:10.3390/ijerph15091881.

Kim, G., Baek, I., Stocker, M. D., Smith, J. E., Van Tassell, A. L., Qin, J., Chan, D. E., Pachepsky, Y., & Kim, M. S. (2020). Hyperspectral imaging from a multipurpose floating platform to estimate chlorophyll-a concentrations in irrigation pond water. *Remote Sensing*, *12*, 2070. doi:10.3390/rs12132070.

Knaeps, E., Ruddick, K. G., Doxaran, D., Dogliotti, A. I., Nechad, B., Raymaekers, D., & Sterckx, S. (2015). A swir based algorithm to retrieve total suspended matter in extremely turbid waters. *Remote Sensing of Environment*, *168*, 66–79. doi:10.1016/j.rse.2015.06.022.

Kwon, S., Seo, I. W., Noh, H., & Kim, B. (2022). Hyperspectral retrievals of suspended sediment using cluster-based machine learning regression in shallow waters. *Science of The Total Environment*, *833*, 155168. doi:10.1016/j.scitotenv.2022.155168.

Li, S., Toming, K., Nõges, T., & Kutser, T. (2022). Integrating remote sensing of hydrological processes and dissolved organic carbon fluxes in long-term lake studies. *Journal of Hydrology*, *605*, 127331. doi:10.1016/j.jhydrol.2021.127331.

Liu, R., Kuang, J., Gong, Q., & Hou, X. (2003). Principal component regression analysis with spss. *Computer methods and programs in biomedicine*, *71*, 141–147. doi:10.1016/s0169-2607(02)00058-5.

Ma, R., & Dai, J. (2005). Investigation of chlorophyll-a and total suspended matter concentrations using landsat etm and field spectral measurement in taihu lake, china. *International Journal of Remote Sensing*, *26*, 2779–2795. doi:10.1080/01431160512331326648.

Ma, Y., Song, K., Wen, Z., Liu, G., Shang, Y., Lyu, L., Du, J., Yang, Q., Li, S., Tao, H. et al. (2021). Remote sensing of turbidity for lakes in northeast china using sentinel-2 images with machine learning algorithms. *IEEE Journal of Selected Topics in Applied Earth Observations and Remote Sensing*, *14*, 9132–9146. doi:10.1109/JSTARS.2021.3109292.

Maier, P. M., & Keller, S. (2019). Application of different simulated spectral data and machine learning to estimate the chlorophyll a concentration of several inland waters. In *2019 10th Workshop on Hyperspectral Imaging and Signal Processing: Evolution in Remote Sensing (WHISPERS)* (pp. 1–5). IEEE. doi:10.1109/WHISPERS.2019.8921073.

Maier, P. M., Keller, S., & Hinz, S. (2021). Deep learning with wasi simulation data for estimating chlorophyll a concentration of inland water bodies. *Remote Sensing*, *13*, 718. doi:10.3390/rs13040718.

Novo, E. M. L. M., Steffen, C. A., & Braga, C. Z. F. (1991). Results of a laboratory experiment relating spectral reflectance to total suspended solids. *Remote Sensing of Environment*, *36*, 67–72. doi:10.1016/0034-4257(91)90031-Z.

Olmanson, L. G., Brezonik, P. L., & Bauer, M. E. (2013). Airborne hyperspectral remote sensing to assess spatial distribution of water quality characteristics in large rivers: The mississippi river and its tributaries in minnesota. *Remote Sensing of Environment*, *130*, 254–265. doi:10.1016/j.rse.2012.11.023.

Ouillon, S., Douillet, P., Petrenko, A., Neveux, J., Dupouy, C., Froidefond, J.-M., Andréfouët, S., & Muñoz-Caravaca, A. (2008). Optical algorithms at satellite wavelengths for total suspended matter in tropical coastal waters. *Sensors*, *8*, 4165–4185. doi:10.3390/s8074165.

Palmer, S. C., Kutser, T., & Hunter, P. D. (2015). Remote sensing of inland waters: Challenges, progress and future directions.

Pechar, L. (1987). Use of an acetone: methanol mixture for the extraction and spectrophotometric determination of chlorophyll-a in phytoplankton. *Algological Studies/Archiv für Hydrobiologie, Supplement Volumes*, *46*, 99–117.

Peterson, K. T., Sagan, V., Sidike, P., Cox, A. L., & Martinez, M. (2018). Suspended sediment concentration estimation from landsat imagery along the lower missouri and middle mississippi rivers using an extreme learning machine. *Remote Sensing*, *10*, 1503. doi:10.3390/rs10101503.

Pyo, J. C., Ligaray, M., Kwon, Y. S., Ahn, M.-H., Kim, K., Lee, H., Kang, T., Cho, S. B., Park, Y., & Cho, K. H. (2018). High-spatial resolution monitoring of phycocyanin and chlorophyll-a using airborne hyperspectral imagery. *Remote Sensing*, *10*, 1180. doi:10.3390/rs10081180.

Rodríguez-López, L., Duran-Llacer, I., González-Rodríguez, L., Cardenas, R., & Urrutia, R. (2021). Retrieving water turbidity in araucanian lakes (south-central chile) based on multispectral landsat imagery. *Remote Sensing*, *13*, 3133. doi:10.3390/rs13163133.

Ross, M. R., Topp, S. N., Appling, A. P., Yang, X., Kuhn, C., Butman, D., Simard, M., & Pavelsky, T. M. (2019). Aquasat: A data set to enable remote sensing of water quality for inland waters. *Water Resources Research*, *55*, 10012–10025. doi:10.1029/2019WR024883.

Rubin, H. J., Lutz, D. A., Steele, B. G., Cottingham, K. L., Weathers, K. C., Ducey, M. J., Palace, M., Johnson, K. M., & Chipman, J. W. (2021). Remote sensing of lake water clarity: Performance and transferability of both historical algorithms and machine learning. *Remote Sensing*, *13*, 1434. doi:10.3390/rs13081434.

Ruddick, K., Vanhellemont, Q., Dogliotti, A., Nechad, B., Pringle, N., & Van der Zande, D. (2016). New opportunities and challenges for high resolution remote sensing of water colour. *Proceedings of the Ocean Optics XXIII, Victoria, BC, Canada*, *7*.

Ryan, K., & Ali, K. (2016). Application of a partial least-squares regression model to retrieve chlorophyll-a concentrations in coastal waters using hyper-spectral data. *Ocean Science Journal*, *51*, 209–221. doi:10.1007/s12601-016-0018-8.

Saberioon, M., Brom, J., Nedbal, V., Soucek, P., & Císar, P. (2020). Chlorophyll-a and total suspended solids retrieval and mapping using sentinel-2a and machine learning for inland waters. *Ecological Indicators*, *113*, 106236. doi:10.1016/j.ecolind.2020.1062366.

Sagan, V., Peterson, K. T., Maimaitijiang, M., Sidike, P., Sloan, J., Greeling, B. A., Maalouf, S., & Adams, C. (2020). Monitoring inland water quality using remote sensing: potential and limitations of spectral indices, bio-optical simulations, machine learning, and cloud computing. *Earth-Science Reviews*, *205*, 103187. doi:10.1016/j.earscirev.2020.103187.

Schaeffer, B. A., Schaeffer, K. G., Keith, D., Lunetta, R. S., Conmy, R.,

& Gould, R. W. (2013). Barriers to adopting satellite remote sensing for water quality management. *International Journal of Remote Sensing*, *34*, 7534–7544. doi:10.1080/01431161.2013.823524.

Segl, K., Guanter, L., Rogass, C., Kuester, T., Roessner, S., Kaufmann, H., Sang, B., Mogulsky, V., & Hofer, S. (2012). Eetes — the enmap end-to-end simulation tool. *IEEE Journal of Selected Topics in Applied Earth Observations and Remote Sensing*, *5*, 522–530. doi:10.1109/JSTARS.2012.2188994.

Silveira Kupssinskü, L., Thomassim Guimarães, T., Menezes de Souza, E., C Zanotta, D., Roberto Veronez, M., Gonzaga, L., & Mauad, F. F. (2020). A method for chlorophyll-a and suspended solids prediction through remote sensing and machine learning. *Sensors*, *20*, 2125. doi:10.3390/s20072125.

Song, K., Li, L., Tedesco, L. P., Li, S., Clercin, N. A., Hall, B. E., Li, Z., & Shi, K. (2012). Hyperspectral determination of eutrophication for a water supply source via genetic algorithm–partial least squares (ga–pls) modeling. *Science of the Total Environment*, *426*, 220–232. doi:10.1016/j.scitotenv.2012.03.058.

Menezes de Souza, E., Veronez, R., Gonzaga Jr, L., Mauad, F. et al. (2020). A method for chlorophyll-a and suspended solids prediction through remote sensing and machine learning. *Sensors (Basel, Switzerland)*, *20*. doi:10.3390/s20072125.

Stendera, S., Adrian, R., Bonada, N., Cañedo-Argüelles, M., Hugueny, B., Januschke, K., Pletterbauer, F., & Hering, D. (2012). Drivers and stressors of freshwater biodiversity patterns across different ecosystems and scales: a review. *Hydrobiologia*, *696*, 1–28. doi:10.1007/s10750-012-1183-0.

Sudduth, K. A., Jang, G.-S., Lerch, R. N., & Sadler, E. J. (2015). Long-term agroecosystem research in the central mississippi river basin: Hyperspectral remote sensing of reservoir water quality. *Journal of environmental quality*, *44*, 71–83. doi:10.2134/jeq2014.02.0060.

Thiemann, S., & Kaufmann, H. (2002). Lake water quality monitoring using hyperspectral airborne data—a semiempirical multisensor and multitemporal approach for the mecklenburg lake district, germany. *Remote sensing of Environment*, *81*, 228–237. doi:10.1016/S0034-4257(01)00345-5.

Transon, J., d'Andrimont, R., Maugnard, A., & Defourny, P. (2018). Survey of hyperspectral earth observation applications from space in the sentinel-2 context. *Remote Sensing*, *10*, 157. doi:10.3390/rs10020157.

Van Puijenbroek, P., Evers, C., & van Gaalen, F. (2015). Evaluation of water framework directive metrics to analyse trends in water quality in the netherlands. *Sustainability of Water Quality and Ecology*, *6*, 40–47. doi:10.1016/j.swaqe.2015.02.004.

Vanhellemont, Q., & Ruddick, K. (2021). Atmospheric correction of sentinel-3/olci data for mapping of suspended particulate matter and chlorophyll-a concentration in belgian turbid coastal waters. *Remote Sensing of Environment*, *256*, 112284. doi:10.1016/j.rse.2021.112284.

Vinciková, H., Hanuš, J., & Pechar, L. (2015). Spectral reflectance is a reliable water-quality estimator for small, highly turbid wetlands. *Wetlands Ecology and Management*, *23*, 933–946. doi:10.1007/s11273-015-9431-5.

Wang, J., Shi, T., Yu, D., Teng, D., Ge, X., Zhang, Z., Yang, X., Wang, H., & Wu, G. (2020). Ensemble machine-learning-based framework for estimating total nitrogen concentration in water using drone-borne hyperspectral imagery of emergent plants: A case study in an arid oasis, nw china. *Environmental Pollution*, *266*, 115412. doi:10.1016/j.envpol.2020.115412.

Wold, S., Sjöström, M., & Eriksson, L. (2001). Pls-regression: a basic tool of chemometrics. *Chemometrics and intelligent laboratory systems*, *58*, 109–130. doi:10.1016/S0169-7439(01)00155-1.

Wu, J.-L., Ho, C.-R., Huang, C.-C., Srivastav, A. L., Tzeng, J.-H., & Lin, Y.-T. (2014). Hyperspectral sensing for turbid water quality monitoring in freshwater rivers: empirical relationship between reflectance and turbidity and total solids. *Sensors*, *14*, 22670–22688. doi:10.3390/s141222670.